**Table 1. Pile and soil material properties used in numerical simulation**

| Material | Model | Modulus $E$ (MPa) | Density $\gamma$ (kN/m$^3$) | Poisson's ratio $\upsilon$ | Cohesion $c$ (kPa) | Friction angle $\varphi$ (°) | Lateral coefficient $K_0$ |
|---|---|---|---|---|---|---|---|
| Concrete pile | Isotropic elastic | 20,000 | 25 | 0.2 | | | 1.0 |
| Soft clay | Mohr-Coulomb | 5 | 18 | 0.3 | 3 | 20 | 0.65 |
| Sand | Mohr-Coulomb | 25 | 20 | 0.3 | 0.1 | 45 | 0.5 |

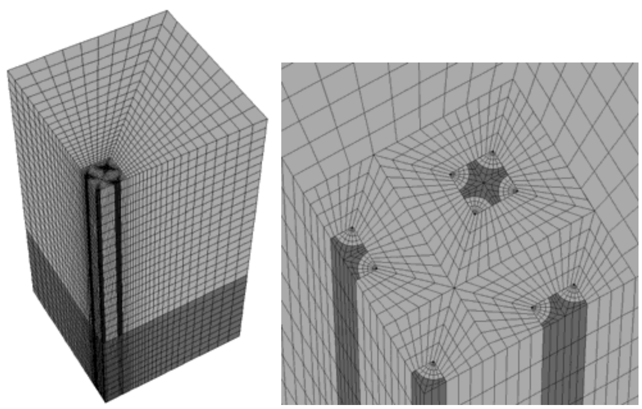

**FIG. 1. Geometric model, and typical finite difference meshes for 3×3 XCC pile group (1/4 model).**

## Large-scale Model Test Summary

Large-scale model test system is composed of test site, loading system and measuring system, etc. The model bank is located in Hohai University, Nanjing, China, and its size is 5 m × 4 m × 7 m (length × width × height).

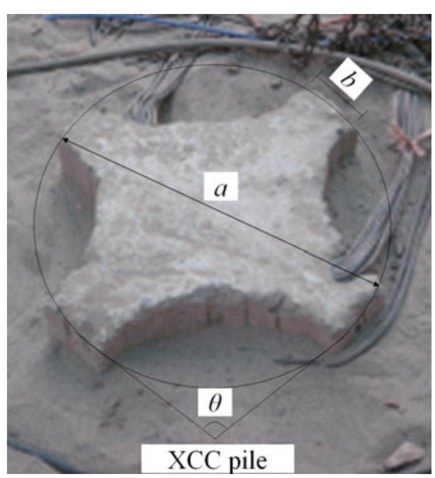


**FIG. 2. The cross-section of the XCC pile for large-scale model test.**

**Table 2. Mechanical parameters of large-scale model test soils**

| Material | Cohesion $c$ (kPa) | Internal friction angle $\varphi$ (°) | Moisture content $\omega$ (%) | Natural density $\rho$ (g.cm$^{-3}$) |
|---|---|---|---|---|
| Clay | 27.6 | 21.2 | 16.7 | 1.9 |
| Sand | 17.6 | 25.9 | 5.1 | 1.5 |

The loading system is composed of hydraulic jack, and reaction beam etc. The measuring system is composed of load cell, reinforcement stress meters, earth pressure cell, frequency instrument and displacement meter, etc. The cross-section of XCC pile is shown in Fig. 2. Table 2 is the mechanical parameters of model test soils.

### Numerical Model Verification

In order to simulate experimental conditions, the size and parameters of numerical model were kept the same as those under experimental conditions (Wang et al. 2010). The load settlement curves ($Q$-$s$) of numerical simulation and measured results are shown in Fig. 3.

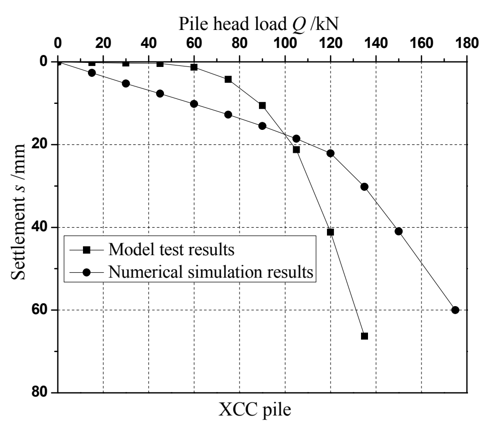


**FIG. 3. The comparison of curves of pile head load versus settlement ($Q$-$s$).**

## INFLUENCING FACTOR ANALYSIS

### Influence Analysis of Pile Positions

Fig. 4 (a) shows that pile top settlement increases with pile head load increasing for each pile in different positions, and the relationships are nearly linear. Under the same loading grade, the settlement of interior pile is smaller than that of edge pile and corner pile. It may be because the masking effect of pile-pile affects interior pile more obviously than edge pile and corner pile. Fig. 4 (b) shows that when piles in different positions (contains single pile), the distributions of pile axial force along pile depth are uniform, and the values of interior pile is smaller than that of edge pile and corner pile.

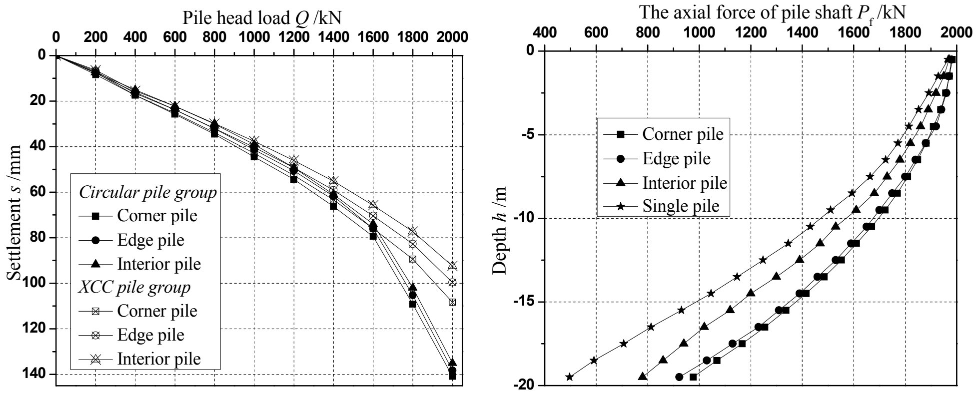

(a) (b)

**FIG. 4. The curves of *Q-s* (a), and distributions of axial force of pile shaft along pile depth (b) under different pile positions.**

## Influence Analysis of the Stiffness of Pile End Soil

Fig. 5 (a) shows that the curves of pile top settlement and pile head load under different modulus ratios of pile side soil with pile end soil are uniform, and the settlement increases with load increasing. Fig. 5 (b) shows that the distributions of the axial force of pile shaft along pile depth under 1200 kN pile head load are uniform, and the pile shaft friction develops more fully when pile end soil becomes less stiff.

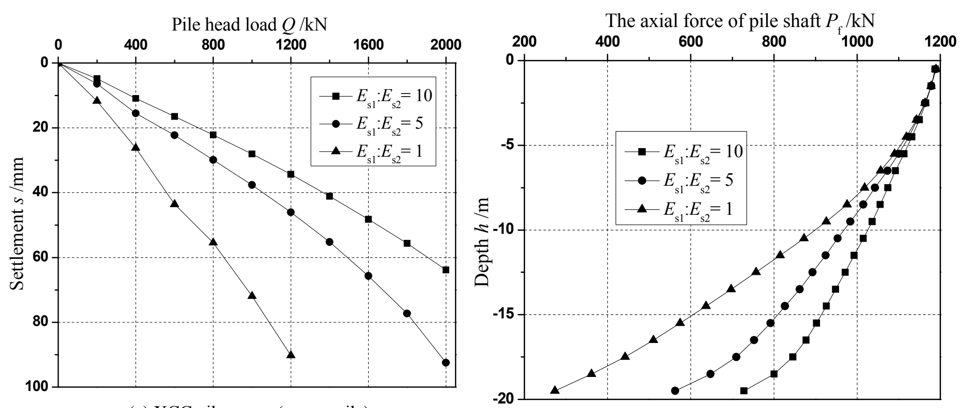

(a) XCC pile group (corner pile) (b) XCC pile group (corner pile)

**FIG. 5. The curves of *Q-s* (a), and distributions of axial force of pile shaft along pile depth (b) under different soil modulus ratios.**

## Influence Analysis of the Modulus of Pile

Fig. 6 (a) shows that the distributions of the axial force of pile shaft along pile depth under different pile head load are uniform, and increases with load increasing. Fig. 6 (b) shows that the distributions of the axial force of pile shaft along pile depth under 1400 kN pile head load are uniform, and the values are approximately equal. Fig. 7 (a) shows that the curves of pile top settlement and pile head load under different friction coefficient of pile-soil are uniform, and the ultimate capacity increases with friction coefficient of pile-soil increasing. Fig. 7 (b) shows that the distributions of the axial force of pile shaft along pile depth with different friction coefficient of pile-soil under 1400 kN pile head load are uniform, and the values are approximately equal.

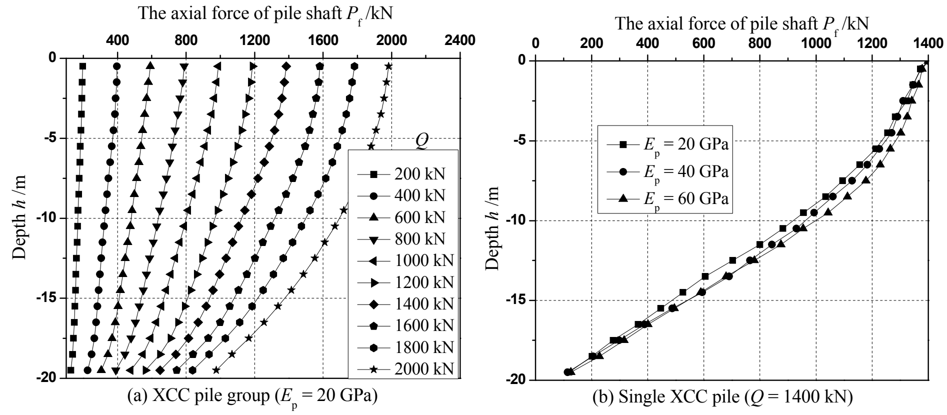


**FIG. 6. The distributions of axial force of pile shaft along pile depth under different load (a), and under different pile modulus (b). Influence Analysis of the friction coefficient of pile-soil**

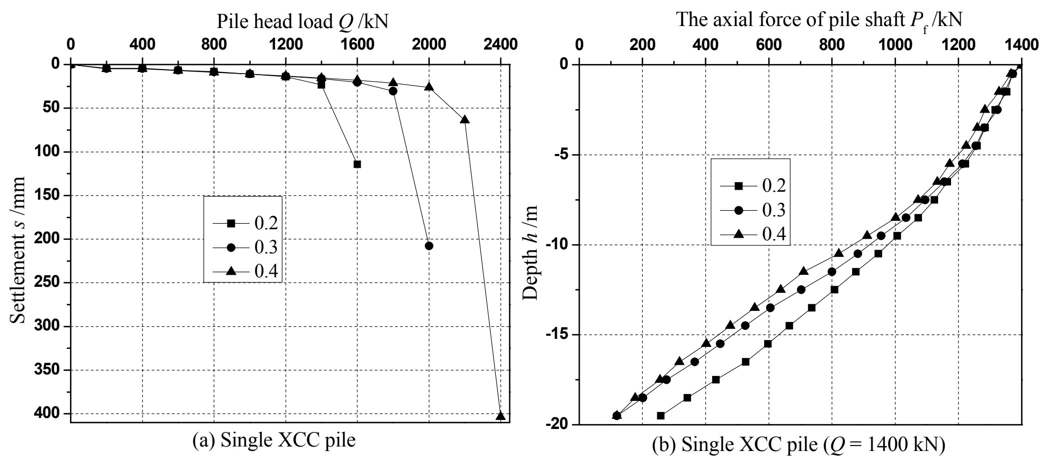


**FIG. 7. The curves of *Q-s* (a), and distributions of axial force of pile shaft along pile depth (b) under different friction coefficient of pile-soil.**

## CONCLUSIONS

Based on a series of numerical studies presented in this paper, the following conclusions can be drawn:

The distributions of axial force of pile shaft and compressive capacity of XCC pile group are similar to those of circular pile group, and the values are larger.

The compressive capacity of XCC pile group increases with the increasing of stiffness of pile end soil, the increasing of pile modulus, and the increasing of friction coefficient of pile-soil.

These conclusions obtained in this study will be helpful to practicing engineers using XCC pile this new technology.

## ACKNOWLEDGMENTS

The authors appreciate the support of the National Natural Science Foundation of Hohai University (No. 2009423711), the China Postdoctoral Science Foundation funded project (No. 20090461062), and the Fundamental Research Funds for the Central Universities (No. 2009B14514).

## REFERENCES

Chen, Y.M., Liu, H.L. and Kong, G.Q. (2010). "Development and application for X-section cast-in-place concrete pile." Proceedings of the 4th Japan-China Geotechnical Symposium, Okinawa, pp: 389-392.

Lei, G.H. (2001). "Behavior of excavated rectangular piles (barrettes) in granitic saproletes." Hong Kong: The Hong Kong University of Science and Technology.

Liu, H.L. (2010). "X-section cast-in-place reinforced concrete pile construction method." China patent: ZL 200710020306.3. (in Chinese)

Liu, H.L. (2008). "X-section cast-in-place reinforced concrete pile sinking model system." China patent: ZL200720036892.6. (in Chinese)

Liu, H.L., Liu, Z.P. and Wang, X.Q. (2009). "Study on the geometric characteristics of the cast-in-place X-type vibro-pile section." *China Railway Science*, Vol. 30(1): 17-23. (in Chinese)

Liu, Z.P. (2008). "Research on bearing behavior of X-shaped concrete pile." Nanjing: Hohai University. (in Chinese)

Wang, Z.Q., Liu, H.L., Zhang, M.X., et al. (2010). "Full scale model tests on vertical bearing characteristics of cast-in-place X-section pile." *Chinese Journal of Geotechnical Engineering*, Vol. 32(6): 903-907. (in Chinese)

Wang, X.Q., Chen, Y.H., Lin, F. and Lu, X.Y. (2008). "Study on ultimate bearing capacity of Y-shaped vibro-pile." *Journal of Central South University of Technology*, Vol. 15(2): 186-194.

Wang, X.Q. (2009). "Bearing behavior and design method research of Y-section pile." Nanjing: Hohai University. (in Chinese)

Yuan, J. (2009). "Research on the full-scale model test for the behavior of X-section pile under lateral load." Nanjing: Hohai University. (in Chinese)

# The Bearing Behavior of Foundation Pile Evaluated by the Mesh Free Local Petrov-Garlerkin Method

He Wei[1]

[1]Associate professor, Institute of geotechnical engineering, Changsha University of Science & Technology, Wanjialinan Road No. 960, Changsha, Hunan Province, P.R.China, 410004. E-mail: heweicslg@yahoo.com.cn

## ABSTRACT

In this paper, a kind of the Mesh free method was utilized to conduct a series of computational modeling to evaluate the bearing behavior of extended-length piles. The computational program code and boundary conditions were generated based on the elastic-plastic behavior of the surrounding soil, reinforcements, and the non-continuous interface between the piles and the soil. This was then verified with the Marc (a commercial available software package) by analyzing a classical mechanics problem. Lastly, the bearing capacity and response behavior of long-length bridge pile were analyzed including the relationship between the piles length-diameter ratio, pile settlement, and the non-linear behavior of the load-settlement curve. Overall, the results indicated that the optimal length of the pile is directly related to the stiffness of the soil, i.e., the stiffer the soil, the longer the allowable pile length.

## INTRODUCTION

Although a lot of research has indicated that the extended-length and large-diameter piles are usually of high ultimate bearing capacity for deeper penetration depths, the allowable bearing capacity of these piles is better determined by the settlement limitation method (Zhao, 2004, 2006; Liu, 2004; Feng, 2005; Zhong, 2005).Thus, it is of great significance to accurately predict and model the load-settlement curve so that a rational allowable bearing capacity can be determined. Four different theories and analysis methods are often used for pile settlement analysis, namely: the load transfer, the elastic mechanics, the numerical, and the empirical method, respectively.

One of the commonly used numerical analysis methods in engineering applications is the finite element method (FEM). However, the FEM establishes its discrete equations based on the grid method, which is often associated with poorly distorted elements and boundary conditions, thus resulting in noticeable errors particularly when solving large deformation problems.

To overcome some of these limitations, the Meshfree method was formulated (Pang, 1999; Li, 2001; Liu, 2003). Unlike the FEM, the Meshfree method establishes its approximate functions based on nodes and not grids; thus, the level of accuracy can be enhanced because there is no need to generate grids and do a re-mesh modeling. Accordingly, the Meshfree Local Petrov-Garlerkin method (MLPG) was utilized in this study to evaluate the bearing capacity and response behavior of extended-length piles. Results of these numerical analyses are presented and discussed in this paper.

## THE ELASTO-PLASTIC MLPG METHODS

### The Weighted Residual Method

A piles problem can be categorized as a typical solid mechanics problem, which can be modeled using basic mechanics equations but taking into account the necessary boundary conditions. In general, the unknown function of a structure or an element should follow the basic equilibrium rules as follows:

$$\mathbf{A}[\mathbf{u}(\mathbf{x})]=\begin{Bmatrix} A_1[\mathbf{u}(\mathbf{x})] \\ A_2[\mathbf{u}(\mathbf{x})] \\ \vdots \\ A_{m_1}[\mathbf{u}(\mathbf{x})] \end{Bmatrix}=0 \quad (\text{ in domain } \Omega) \tag{1}$$

With the boundary conditions given as：

$$\mathbf{B}[\mathbf{u}(\mathbf{x})]=\begin{Bmatrix} B_1[\mathbf{u}(\mathbf{x})] \\ B_2[\mathbf{u}(\mathbf{x})] \\ \vdots \\ B_{m_2}[\mathbf{u}(\mathbf{x})] \end{Bmatrix}=0 \quad (\text{ on boundary } \Gamma) \tag{2}$$

Where $\Gamma$ is the boundary condition of $\Omega$ and $\mathbf{x}=[x, y, z]^T$ is the arbitrary nodal point of analysis. The unknown function $\mathbf{u}(\mathbf{x})$ may be a vector field of several variables and it is often molded using a displacement variable. The equivalent integral form of the differential Equations (1) and (2) is:

$$\int_\Omega \mathbf{v}^T \mathbf{A}[\mathbf{u}(\mathbf{x})]d\Omega+\int_\Gamma \overline{\mathbf{v}}^T \mathbf{B}[\mathbf{u}(\mathbf{x})]d\Gamma=0 \tag{3}$$

Where $\mathbf{v}$ and $\overline{\mathbf{v}}$ are the test and weight functions, respectively, and they are of the $m_1$th and $m_2$th order, respectively. The equivalent weak form can then be obtained through the partial integration of Equation (3):

$$\int_\Omega \mathbf{C}(\mathbf{v}^T)\mathbf{D}[\mathbf{u}(\mathbf{x})]d\Omega+\int_\Gamma \mathbf{E}(\overline{\mathbf{v}}^T)\mathbf{F}[\mathbf{u}(\mathbf{x})]d\Gamma=0 \tag{4}$$

## The Moving Least Squares Method

Assume that $u(\mathbf{x})$ is the unknown function defined in the domain $\Omega$, while the function value on N nodes (denoted as $x_I$ and $I$=1, 2, ...,$N$) in the domain is known as $u_I = u(\mathbf{x}_I)$. If x is the point of analysis in the domain, then the approximation function value at point x can be expressed as follows:

$$u^{\mathrm{h}}(\mathbf{x},\mathbf{x}_{\mathrm{I}}) = \mathbf{p}^{\mathrm{T}}(\mathbf{x}_{\mathrm{I}})\mathbf{a}(\mathbf{x}) \quad , \quad I = 1,2,...,n \tag{5}$$

Where $p_i(\mathbf{x}_I)$ is the basis function and $\mathbf{a}(\mathbf{x})$ is the coefficient matrix, which can be expressed as:

$$\mathbf{a}(\mathbf{x})=[a_1(\mathbf{x}), a_2\,(\mathbf{x}),\ldots, a_m\,(\mathbf{x})]^{\mathrm{T}} \tag{6}$$

Where $a_i(\mathbf{x})$ are the undetermined coefficients related to x and $m$ is the number of the basic functions. The basis function has the simplest form as a 1st order single-type equation, and its polynomial basis function can be written as follows:

$$\mathbf{p}^{\mathrm{T}}(\mathbf{x}) = \mathbf{p}^{\mathrm{T}}(x, y) = [1, x, y, xy, x^2, y^2, ..., x^m, y^m] \tag{7}$$

Local approximation functions can then be obtained using Equation (8)

$$u^{\mathrm{h}}(\mathbf{x},\mathbf{x}_I) = \mathbf{p}^{\mathrm{T}}(\mathbf{x}_{\mathrm{I}})\mathbf{A}^{-1}(\mathbf{x})\mathbf{B}(\mathbf{x})\mathbf{u} = \sum_{I=1}^{N} N_{\mathrm{I}}(\mathbf{x})u_{\mathrm{I}} = \mathbf{N}^{\mathrm{T}}(\mathbf{x})\mathbf{u} \tag{8}$$

Where $N_I$ is the shape function, with its specific form written as follows:

$$N_{\mathrm{I}}(\mathbf{x}) = \mathbf{p}^{\mathrm{T}}(\mathbf{x}_{\mathrm{I}})\mathbf{A}^{-1}(\mathbf{x})\mathbf{B}(\mathbf{x}) \tag{9}$$

The $\mathbf{N}$ represents the matrix of the shape functions, whose specific form is given as follows:

$$\mathbf{N} = \mathbf{P}^{\mathrm{T}}\mathbf{A}^{-1}(\mathbf{x})\mathbf{B}(\mathbf{x}) = [N_1, N_{2,\ldots}N_{\mathrm{N}}] \tag{10}$$

$$\mathbf{A}(\mathbf{x}) = \sum_{I=1}^{N} \omega_{\mathrm{I}}(|\mathbf{x}-\mathbf{x}_{\mathrm{I}}|)\mathbf{p}(\mathbf{x}_{\mathrm{I}})\mathbf{p}^{\mathrm{T}}(\mathbf{x}_{\mathrm{I}}) = \mathbf{P}^{\mathrm{T}}\mathbf{W}(|\mathbf{x}-\mathbf{x}_{\mathrm{I}}|)\mathbf{P} \tag{11}$$

$$\begin{aligned}\mathbf{B}(\mathbf{x}) &= [\mathbf{B}_1, \mathbf{B}_2, \ldots, \mathbf{B}_{\mathrm{N}}] \\ &= [\omega_1(|\mathbf{x}-\mathbf{x}_{\mathrm{I}}|)\mathbf{p}(\mathbf{x}_1), \omega_2(|\mathbf{x}-\mathbf{x}_{\mathrm{I}}|)\mathbf{p}(\mathbf{x}_2), \ldots, \omega_{\mathrm{N}}(|\mathbf{x}-\mathbf{x}_{\mathrm{I}}|)\mathbf{p}(\mathbf{x}_{\mathrm{N}})] = \mathbf{P}^{\mathrm{T}}\mathbf{W}(|\mathbf{x}-\mathbf{x}_{\mathrm{I}}|)\end{aligned} \tag{12}$$

Where ω is the weight function that controls the supporting domain.

## The Discretization of the Basic Equation of MLPG

When calculating the discrete basic equation of MLPG, the residual error should be zero in the *r* local domain $\Omega_i$ and boundary $\Gamma_i$. In theory, the mechanics equilibrium conditions and boundary conditions are satisfied once the modeling domain is covered by the union of *r* local domain $\Omega_i$. However, Atluri (1998) pointed out that desirable results could be obtained even if the conditions are not fully satisfied. The test and trial functions are selected from a different function space and the corresponding equivalent integral form is given as follows:

$$\int_{\Omega_i} \mathbf{W}_i^{\mathrm{T}} \mathbf{A} \left[ \sum_{j=1}^{N} \mathbf{N}_j(\mathbf{x}) \mathbf{u}_j \right] \mathrm{d}\Omega_i + \int_{\Gamma_i} \bar{\mathbf{W}}_i^{\mathrm{T}} \mathbf{B} \left[ \sum_{j=1}^{N} \mathbf{N}_j(\mathbf{x}) \mathbf{u}_j \right] \mathrm{d}\Gamma_i, \qquad i = 1, 2, \ldots, r \tag{13}$$

Where $\Gamma_i = \partial\Omega_i \cup L_i$ is the boundary of a local domain $\Omega_i$, $\partial\Omega_i$ is part of the boundaries $\Gamma$ right in the local domain (meaning $\partial\Omega_i = \Gamma_i \cap \Gamma$), and $L_i$ is the rest of the boundaries besides $\partial\Omega_i$ (as shown in Fig. 1). Boundary conditions are then determined on $\partial\Omega_i$ not on $L_i$. For a local domain, which is totally in the global domain, there are no intersections between $\Gamma_i$ and $\Gamma$, then $\partial\Omega_i = \varnothing$, and $\Gamma_i = L_i$. The local domain $\Omega_i$ can then be selected as a circle, an ellipse, or a rectangle for a two-dimensional analysis.

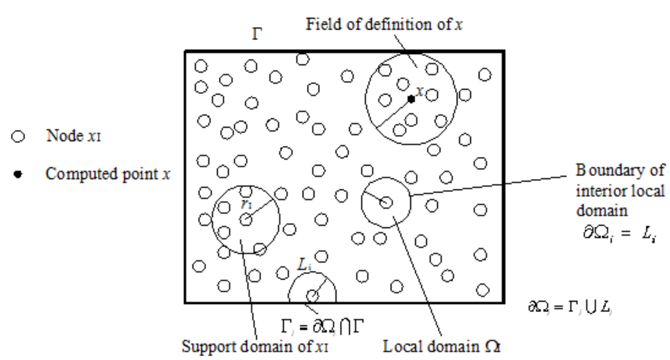


**Fig.1. Schematic of the Local Domain and Boundaries.**

The equivalent weak form can be obtained by partial integration of Equation (13) to Equation (14) as follows:

$$\int_{\Omega_i} C\left(\mathbf{W}_i^{\mathrm{T}}\right) D \left[ \sum_{j=1}^{N} \mathbf{N}_j(\mathbf{x}) \mathbf{u}_j \right] \mathrm{d}\Omega_i + \int_{\Gamma_i} E\left(\bar{\mathbf{W}}_i^{\mathrm{T}}\right) F \left[ \sum_{j=1}^{N} \mathbf{N}_j(\mathbf{x}) \mathbf{u}_j \right] \mathrm{d}\Gamma_i, \qquad i = 1, 2, \ldots, r \tag{14}$$

Equations (13) or (14) represents the *r* set of equations, and if r = N, then the quantity of the local-domain is equal to the nodes. Then, the N undetermined coefficients can be easily solved; otherwise, if r> N, the minimum square method should be introduced.

### The Elastic-Plastic Behavior of Materials

In the elasto-plastic model, the total deformation is divided into two parts; the elastic deformation that follows Hook's law and the plastic deformation that follows plastic deformation. Three assumptions should be made in modeling the plastic deformation: 1) the failure criteria, 2) the hardening law, and 3) the flow rule. These three assumptions differ with the elasto-plastic model. Due to similarity with FEM, details of these assumptions are not shown in this paper [Xu, 1995].

## THE INTERFACE BETWEEN PILES AND SOIL

In piling and soil mechanics engineering, inhomogeneous materials should be taken into account when considering piles and soil interaction, which causes discontinuity in the derivation of the displacement function. The traditional FEM deals with this problem by generating grids and setting the grid interface to overlap the physical interfaces. However, there are no grids generated in the Meshfree method, so a new approach should be introduced to take into account these aspects.

Cordes (1998) proposed a simplified approach to deal with inhomogeneous materials; namely the visibility criteria. In the calculation process, a program should check out what kind of material the calculation point x belongs to. Then, a circular domain of influence with radius $r_{mI}$ is employed to find the nodes in it. The influence of the nodes, which are both in the influence domain and the same material as point x, will be taken into account to approximate the displacement at point x, as shown in Fig. 2.

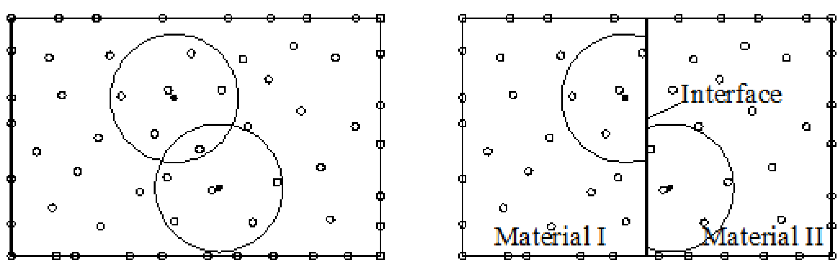


(*a*) Homogeneous materials ; (*b*) Inhomogeneous materials

**Fig.2. The Influencing Domain in Homogeneous and Inhomogeneous Materials.**

The trial function, test function, and their derivatives follow these rules and are discontinuous on the interfaces between different materials, so the following constraint conditions should be applied to the interface $\Gamma_s$ :

$$\int_{\Gamma_s} (\mathbf{u}^+ - \mathbf{u}^-) d\Gamma = 0 \qquad (15)$$